A compact wideband printed inverted-F antenna for smart-card-sized IoT devices

Thi Xuan Dang, Quoc Thuc Nguyen, Van Lam Phi, Quang Khai Trinh, Thi Lan Tran*

Faculty of Electrical and Electronic Engineering, University of Transport and Communications, Hanoi, Vietnam
**Corresponding author E-mail: ttlan@utc.edu.vn*
DOI: https://doi.org/10.64032/mca.v30i3.416

Abstract

A compact printed Inverted-F antenna (PIFA) with a wide impedance bandwidth is proposed for integration into 53.98 × 85.6 mm² smart-card–sized IoT devices. The antenna occupies only 14 × 31.1 mm² and achieves a wide impedance bandwidth by introducing an F-shaped parasitic stub, which generates a controlled dual-resonant response. A prototype was fabricated on a single-layer FR-4 substrate (εr = 4.3, thickness of 1 mm) using standard PCB etching. Measurements show a −10 dB bandwidth of 540 MHz (2.12–2.66 GHz), which agrees well with simulations and validates the robustness of the dual-mode mechanism. The antenna exhibits a peak gain of 3.69 dBi and a radiation efficiency of 93.7% at 2.4 GHz. Compared with recent PIFA and parasitic-element-based structures in the literature, the proposed design provides competitive or superior bandwidth while maintaining a simple planar profile and extremely compact footprint without using defected ground structures, multilayer substrates, tunable components, or metamaterial loading. These characteristics make the proposed antenna suitable for cost-effective and space-constrained IoT terminals operating in the 2.4 GHz band.

Keywords*: Internet of things; Parasitic element; Printed inverted-F antenna; Smart-card-sized electronics; Wideband antenna.*

Abbreviations

DGS	Defected ground structures
IoT	Internet of Things
PIFA	Printed Inverted-F antenna
PCBs	Printed circuit boards
SMA	SubMiniature version A

1. Introduction

The rapid growth of wireless and Internet of Things (IoT) technologies has driven an increasing demand for compact, wideband, and cost-effective antennas. Among various candidates, the Printed Inverted-F Antenna (PIFA) has emerged as a promising solution due to its compact size, low-profile structure, ease of fabrication, and high compatibility with printed circuit boards (PCBs), while maintaining stable radiation performance [1].

Modern IoT devices such as wearables, embedded sensors, and small-sized wireless modules are increasingly being miniaturized and are often comparable in size to smart cards. These platforms typically integrate the antenna alongside transceiver circuits, power units, sensors, and controllers on a single plane, leaving limited space for antenna placement [2]. As the integration density increases, frequency deviation caused by electromagnetic coupling with neighboring components becomes a critical issue, directly affecting impedance matching and radiation performance.

The study presented in [3] analyzed the allocation of antenna area in smart card-sized devices and recommended dedicating approximately one quarter of the total area to the antenna to ensure adequate performance. However, the design in [3] mainly focuses on antenna size optimization, while the impedance bandwidth remains relatively narrow. As a result, the antenna can be highly susceptible to frequency detuning when integrated into complex circuit environments, which may significantly degrade impedance matching and radiation performance. Therefore, achieving a wide impedance bandwidth becomes a key design objective in this work. A wider bandwidth not only ensures full coverage of the 2.4 GHz ISM band but also enhances tolerance to frequency detuning caused by electromagnetic coupling and fabrication variations, thereby improving robustness in practical IoT environments [4].

To overcome these challenges, several bandwidth-enhancement techniques for PIFA structures have been investigated, including:

- The use of parasitic elements [5].
- Slot loading on the radiating element or ground plane [6].
- Implementation of defected ground structures (DGS) [11].
- Geometric optimization through meandering or fractal designs [12].

Each technique has certain trade-offs and should be carefully considered during the antenna design process. The use of parasitic elements enables multi-resonance characteristics without significantly increasing antenna size; however, it requires precise control of electromagnetic coupling. Slot-loading extends the surface current path to improve bandwidth but may complicate fabrication and reduce mechanical strength. Defected ground structures (DGS) can enhance impedance bandwidth but may introduce back radiation and efficiency degradation if not properly designed. In addition, geometric techniques such as meandered or fractal structures support size reduction but often increase design complexity and may distort radiation characteristics.

Accordingly, although various bandwidth enhancement techniques have been reported, existing designs still face several limitations, such as increased structural complexity, degraded radiation performance, or limited suitability for highly compact platforms. In particular, the PIFA design in [3], while suitable for small devices, exhibits relatively narrow impedance bandwidth and is therefore more susceptible to frequency detuning in practical environments where strong

Received: 12 February 2026; Revised: 1 April 2026; Accepted: 1 June 2026.

electromagnetic coupling may occur. These limitations highlight the need for a compact antenna solution that can achieve wider bandwidth while preserving stable radiation characteristics and ease of integration. Accordingly, the proposed design focuses on enhancing impedance bandwidth while maintaining compact size and stable radiation performance.

The proposed antenna is developed for compact and low-cost IoT applications operating in the 2.4 GHz ISM band. Recent studies have shown that IoT antenna design requires a trade-off between miniaturization, bandwidth, and radiation efficiency, with typical efficiency ranging from 70% to 85% for FR-4 based structures [9], [10]. Based on these considerations, the design specifications are defined as follows. The antenna is centered at 2.4 GHz and is designed to achieve an absolute impedance bandwidth of approximately 500 MHz ($|S11| < -10$ dB), ensuring full coverage of the 2.4 GHz ISM band. A minimum realized gain of 2–3 dBi is targeted to support reliable short-range wireless communication. In addition, the radiation efficiency is required to be higher than 80% within the operating band, which is consistent with reported performance levels of compact IoT antennas [9]. Furthermore, the antenna exhibits near-omnidirectional radiation characteristics, which are desirable for stable connectivity in practical IoT deployments. The proposed design achieves a balanced trade-off between performance, compactness, and implementation cost.

In practical applications, it is suitable for integration into compact IoT platforms such as smart-card-type devices, wearable sensors, and embedded wireless modules, where space constraints and mutual coupling effects are critical considerations.

2. Design principle of the proposed antenna

This work employs a quarter-wavelength (λ/4) Printed Inverted-F Antenna (PIFA) based on [3]. It comprises a radiating patch on a PCB, a shorting pin to the ground plane, and a feed point. As shown in Fig. 1(a), the design occupies only one quarter of a standard smart card, making it suitable for compact wireless applications. To improve impedance matching and extend the bandwidth, an F-shaped parasitic stub is integrated into the structure, as illustrated in Fig. 1(b). This element modifies the effective electrical length and excites additional resonant modes, resulting in enhanced bandwidth performance. The detailed geometry and dimensions are presented in Fig. 1(c).

The impact of the parasitic stub geometry on the reflection coefficient is illustrated in Fig. 2. Variations in T_4 and L_1 shift the resonance away from the target frequency of 2.4 GHz. Increasing T_4 improves radiation efficiency and gain (3.57–3.70 dBi), as shown in Fig. 3(a), but suppresses the secondary resonance, narrowing the impedance bandwidth. In contrast, decreasing T_4 reduces efficiency and gain significantly, with only a minor effect on the bandwidth.

The parameter L_2 strongly affects the resonant behavior, as shown in Fig. 2. An optimal value of 12 mm yields a clear dual-resonance with good matching and wide impedance bandwidth. Reducing L_2 (e.g., 10 mm) shortens the parasitic branch, ctausing an electrical length mismatch with the main branch. This shifts the secondary resonance to higher frequencies and degrades S_{11}, particularly in the 2.8–3.0 GHz range. In contrast, increasing L_2 (e.g., 14 mm) shifts it to lower frequencies, where it merges with the primary resonance around 2.4 GHz, narrowing the bandwidth. Proper selection of L_2 is therefore required to maintain distinct dual-resonance and achieve optimal performance.

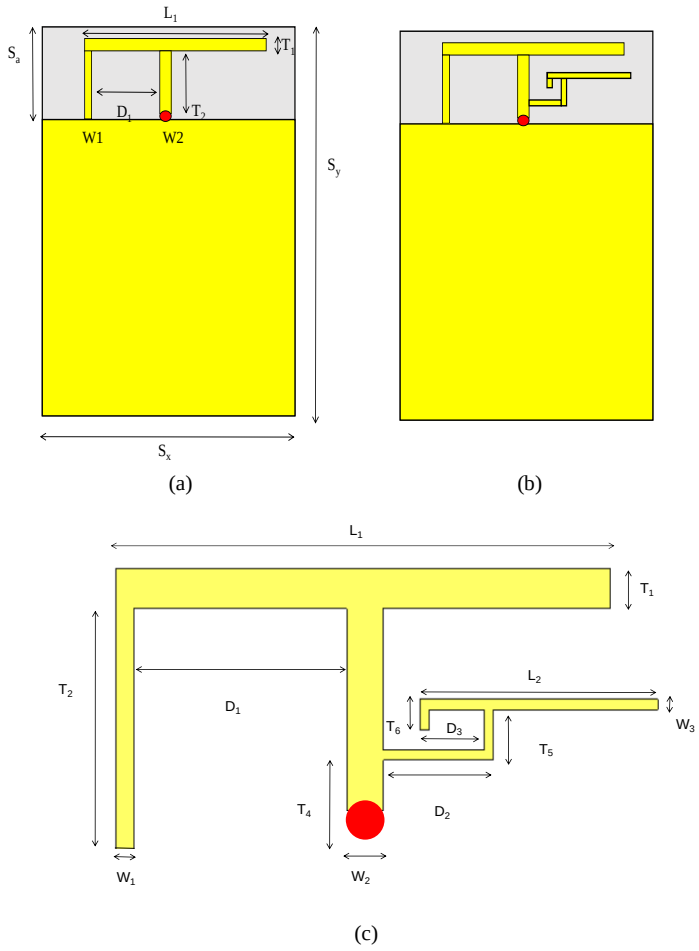


Figure 1: The structure of the proposed antenna: (a) The top view of the PIFA antenna in [3] (S_a/S_y = 1/4), (b) Top view of the proposed antenna, and (c) The antenna with a parasitic stub in detail.

Table 1: Dimension parameters of the proposed antenna.

Para.	L_1	W_3	T_4	T_5	T_6	D_2	D_3	L_2	T_2
Dimension [mm]	27	2	4.5	2.5	1.5	6	4	12	14

Variation of T_5, which sets the vertical length of the folded stub, primarily controls the main resonance at 2.4 GHz. A large value (e.g., 4.5 mm) brings the parasitic stub too close to the main branch, leading to excessive coupling and current distortion, which degrade S_{11} and reduce radiation efficiency (≈59%), as illustrated in Fig. 3(b). Decreasing T_5 improves the response, with an optimal value of 2.5 mm providing wide impedance bandwidth, high efficiency (93.7%), and a maximum realized gain of 3.69 dBi at this frequency. However, a smaller value (e.g., 1.5 mm) shifts the resonance to lower frequencies and weakens the coupling required to sustain the secondary mode, eliminating it and narrowing the bandwidth.

The effect of D_2 on S_{11} is shown in Fig. 2(c). At D_2 = 6 mm, the antenna achieves optimal performance, with a clear resonance at 2.4 GHz (S_{11} < –20 dB) and an additional higher-frequency resonance around 2.6–2.7 GHz, resulting in bandwidth enhancement. For smaller values (e.g., 4 mm), strong coupling between the main radiator and the parasitic stub introduces excessive capacitive interaction, causing frequency detuning and degraded impedance matching. On the other hand, increasing D_2 (e.g., 8 mm) weakens the coupling, reducing excitation of the parasitic mode and consequently degrading the matching performance. Therefore, an appropriate value of D_2 is required to balance the coupling strength and maintain a stable dual-resonance characteristic.

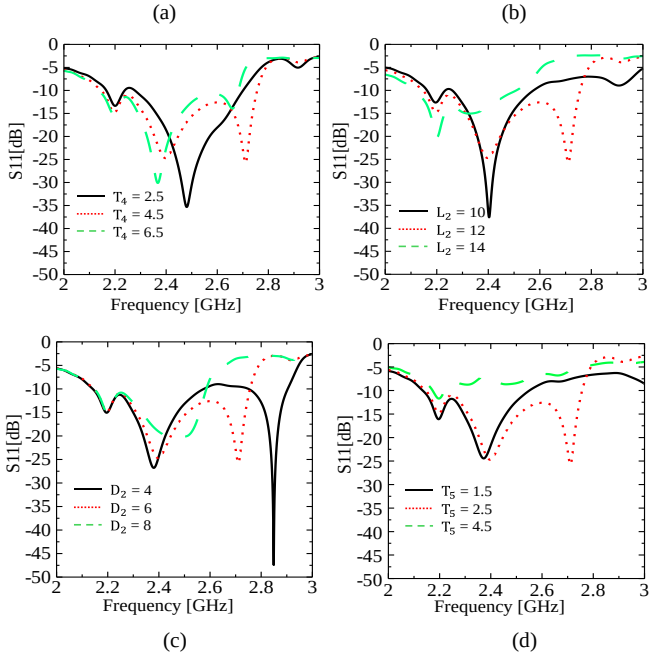


Figure 2. Effect of dimensional parameters on the reflection coefficient: (a) T_4, (b) L_2, (c) D_2 and (d) T_5.

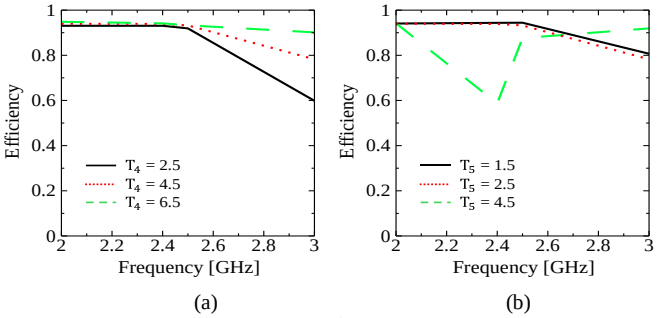


Figure 3. Radiation efficiency versus frequency: (a) T_4, (b) T_5.

Finally, the fine-tuning parameters D_3, T_6, and W_3, although not directly controlling the main resonance, affect the depth and position of the secondary resonance and the smoothness of the S_{11} curve. These elements reduce ripples, stabilize radiation efficiency, and improve impedance matching.When properly adjusted together with L_2, T_5, and D_2, they contribute to overall optimization of the antenna performance and bandwidth. The optimized values are summarized in Table 1.

The surface current distributions at 2.2 GHz, 2.4 GHz, and 2.72 GHz, as shown in Fig. 4, provide a clear physical interpretation of the dual-resonant mechanism. At 2.2 GHz, the current distribution follows a similar pattern to that at 2.4 GHz, being mainly concentrated along the main radiating branch, but with lower intensity and weaker localization around the feed and shorting pin. This indicates that the structure is in a pre-resonant state, where the effective electrical length of the main radiator is not fully satisfied, resulting in poor impedance matching, as also observed in the S_{11} response in Fig. 5. At 2.4 GHz, a strong and well-localized current distribution appears along the main radiating branch, particularly near the feed and shorting pin. This confirms that the main radiator operates as a quarter-wavelength-like resonant structure, where its effective electrical length is approximately $L_1 \approx \lambda/4$ at the fundamental resonance. This mode is directly excited by the feed–shorting configuration and represents the primary resonant mode of the PIFA. A higher-order resonance at 2.72 GHz is primarily concentrated on the F-shaped parasitic stub, indicating the excitation of an additional resonant path with a shorter effective electrical length. This parasitic element behaves as a weakly coupled resonator, which is not directly fed but is excited through near-field capacitive coupling with the main radiating branch.

From an electromagnetic perspective, the proposed structure can be interpreted as a coupled dual-resonator system consisting of the main radiator and the parasitic stub. The coupling occurs primarily at their junction region and is controlled by the spacing D_2, which governs the strength of capacitive interaction and energy transfer between the two resonant paths. When D_2 is properly optimized, sufficient coupling is achieved to excite the secondary resonant mode while preserving the integrity of the fundamental resonance. The first resonant mode is therefore associated with the main $\lambda/4$ radiator (L_1), while the second resonant mode is associated with the parasitic stub (L_2), which introduces an additional resonant path due to its shorter electrical length. The parametric results in Fig. 2(b) further confirm this mechanism, as variations in L_2 directly tune the position of the higher-frequency resonance. Overall, the combination of these two weakly coupled resonant modes results in the dual-resonant S_{11} response shown in Fig. 5(a), thereby enabling the observed bandwidth enhancement.

The simulated performance, including S_{11}, radiation pattern, efficiency, and gain, is summarized in Fig. 5. The reflection coefficient in Fig. 5(a) compares the reference design [3] with the proposed antenna incorporating the F-shaped parasitic stub. The reference achieves a bandwidth of 240 MHz (2.28–2.52 GHz), whereas the proposed design extends it to 600 MHz (2.15–2.75 GHz, 24.5%), mainly due to the introduced coupling that generates two main resonances at 2.4 GHz and 2.72 GHz. The 3D radiation pattern at 2.4 GHz (Fig. 5(b)) shows a nearly omnidirectional characteristic, which is suitable for typical wireless coverage scenarios. The efficiency and gain responses in Fig. 5(c)–(d) remain relatively stable across the operating band, with efficiency above 85% and gain ranging from 1.5 to 3.7 dBi. The peak gain of 3.69 dBi and maximum efficiency of 93.7% indicate that the bandwidth enhancement is achieved without significant degradation in radiation performance.

Overall, the proposed antenna meets the design objectives by providing a bandwidth of approximately 600 MHz (exceeding the 500 MHz target), along with moderate gain (2–3 dBi) and efficiency above 85% across the operating band. These characteristics, enabled by the two main resonances, make the antenna suitable for IoT devices operating in the 2.4 GHz ISM band, particularly compact battery-powered wireless sensor nodes used in applications such as environmental monitoring, smart home systems, and wearable/embedded smart modules, where low power consumption and stable omnidirectional coverage are required.

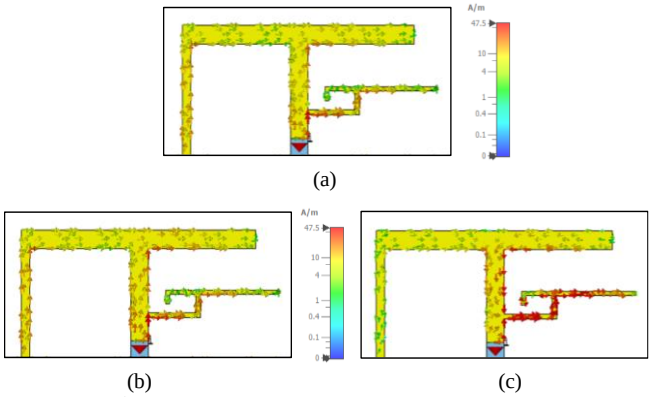


Figure 4. Surface current distribution at (a) 2.2 GHz, (b) 2.4 GHz and (c) 2.72 GHz.

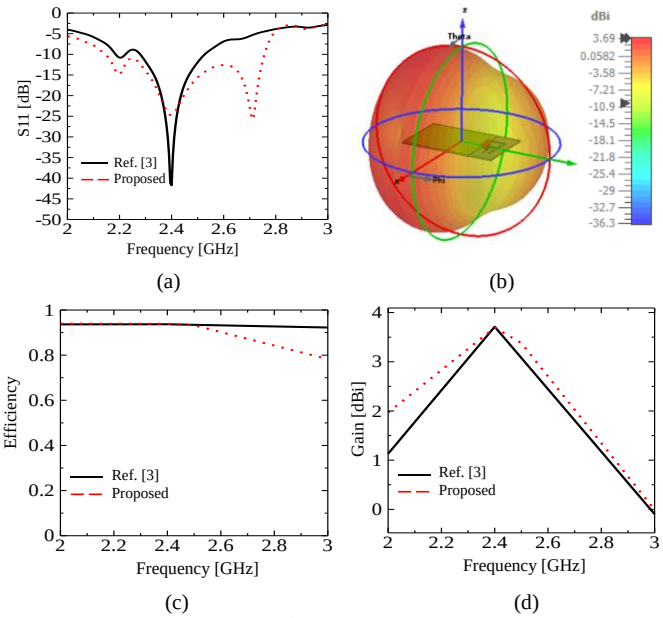


Figure 5. Simulated antenna performance: (a) S_{11}, (b) Radiation patterns, (c) Efficiency, and (d) Gain.

3. Measurement results

To validate the simulation results, a prototype of the proposed antenna was manually fabricated on a single-sided copper-clad FR-4 substrate with a thickness of 1 mm. The fabricated antenna was mounted on a smart-card-sized printed circuit board (53.98 × 85.6 mm²), in which the ground plane was kept identical to the simulated design. The antenna was excited through a 50-Ω SMA connector soldered directly at the feeding point. Photographs of the fabricated prototype are shown in Fig. 5(a) and Fig. 5(b), illustrating the top and bottom views, respectively.

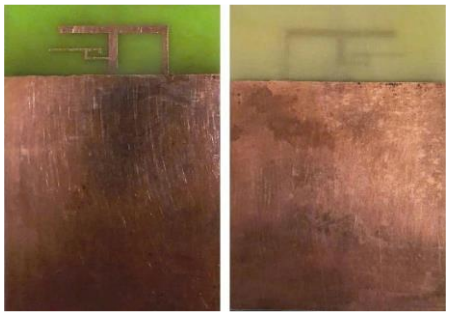


Figure 6. Fabricated antenna prototype: (a) top view and (b) bottom view.

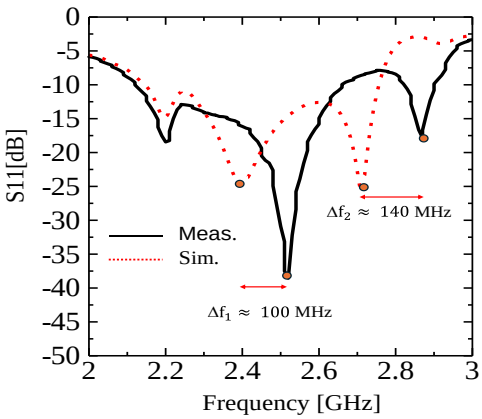


Figure 7. Simulated and measured S11.

The simulated and measured reflection coefficients (S_{11}) of the proposed antenna are presented in Fig. 7. The measured results, obtained using a Keysight E5071C vector network analyzer, indicate that the antenna maintains a wideband operating characteristic after fabrication. Specifically, the −10 dB impedance bandwidth extends from 2.12 to 2.66 GHz, corresponding to an absolute bandwidth of 540 MHz and a fractional bandwidth of approximately 22.6%. In comparison, the simulated results predict a slightly wider bandwidth of 600 MHz (2.15–2.75 GHz), corresponding to a fractional bandwidth of approximately 24.5%. Although a slight reduction is observed in the measured bandwidth, the antenna still fully covers the 2.4 GHz ISM band, thereby satisfying the intended design requirement. Furthermore, as shown in Fig. 7, the measured results exhibit two distinct resonant modes, confirming the multi-resonant operating mechanism of the proposed antenna. A frequency shift is observed compared to the simulated results, particularly for the second resonance around 2.5 GHz. This shift reduces the overlap between the resonances, leading to a slight degradation in the measured impedance bandwidth.

The discrepancies between simulation and measurement are mainly attributed to fabrication tolerances introduced during manual manufacturing and chemical etching, which affect the effective electrical lengths of the radiating and parasitic elements. In addition, the parasitic effects of the SMA connector and the non-ideal dielectric properties of the FR-4 substrate further influence the input impedance characteristics. Despite these discrepancies, the multi-resonant behavior is well preserved, and the fabricated antenna still satisfies the wideband operating requirements over the target frequency

range. These results demonstrate that the proposed antenna exhibits good robustness and practical feasibility under realistic fabrication conditions.

4. Discussion and conclusion

To evaluate the performance of the proposed antenna, a comparison with recently reported designs is summarized in Table 2. The antenna in [11] employs a metamaterial-inspired PIFA structure combined with a defective ground surface (DGS), which enhances radiation characteristics; however, the design introduces additional structural complexity that may complicate fabrication and integration in compact devices. In [12], an evolutionary optimization method is applied to pixelated IFA-inspired antennas, enabling flexible geometry exploration and potential miniaturization. Nevertheless, this approach typically incurs high computational cost and design overhead, limiting its practicality for rapid prototyping. The antenna presented in [13] achieves high radiation efficiency (up to 98%) using an L-shaped microstrip patch configuration. Despite this advantage, its impedance bandwidth is relatively narrow (5.8%), which restricts its suitability for wideband IoT applications in the 2.4 GHz ISM band. In contrast, the work in [14] proposes a compact 3D quasi-isotropic antenna with unique radiation characteristics. However, its limited bandwidth and moderate gain, along with the reliance on non-standard fabrication approaches, may pose challenges for low-cost mass production.

Table 2: A comparison with other studies.

Ref.	Band (GHz)	BW [%]	Gain [dBi]	Size (W × L × H) [mm^3]	Efficiency [%]
[11]	2.4	12.8	4.07	8.3 × 15.3 × 0.5 (RO4350B)	92.2
[12]	2.4	12.9	5.1	9 × 20 × 0.8 (Rogers 5880)	N/A
[13]	2.4	5.8	2.09	28 × 21 ×1.6 (Rogers 5880)	98
[14]	2.4	3.4	1.54	6 × 14 × 20.95 (PLA)	N/A
This work	**2.4**	**24.5**	3.69	14 × 31.1 × 1 (FR-4)	**93.7**

Compared to these designs, the proposed PIFA antenna offers a well-balanced solution, achieving a wide impedance bandwidth of 24.5%, a peak radiation efficiency of 93.7%, and an average efficiency of 85% across the operating band. It features a compact form factor of 14 × 31.1 × 1 mm^3 and employs a straightforward single layer FR-4 substrate, without the need for DGS, fractal elements, or warped geometries. These advantages simplify the fabrication and integration processes, while the measured results further confirm the practical feasibility of the proposed design for modern IoT and wearable wireless applications.

References

[1] Cheung, Y., Yuen, C., and Mung, K. (2018). Miniaturized printed inverted-F antenna for Internet of Things: A design on PCB with a meandering line and shorting strip. International Journal of Antennas and Propagation, 2018, 5172960. https://doi.org/10.1155/2018/5172960

[2] Nguyen Thanh, T., et al. (2025). *A novel energy-efficient health monitoring system with electromagnetic-reducing dual-band antenna*. IEEE Sensors Journal. https://doi.org/10.1109/JSEN.2025.3553929

[3] T. X. Dang, T. T. T. Pham, Q. T. Nguyen, T. L. Tran (2025) An Analysis of the Impact of Ground Plane Sizes on Printed Inverted-F Antennas. The 2025 Asian Workshop on Antennas and Propagation.

[4] Gupta, A., Kansal, A., and Chawla, P. (2022). Design of a wideband patch antenna and performance enhancement using an AMC reflector surface for on-body communication at 2.45 GHz. International Journal of Electronics, 110(6), 1121–1136. https://doi.org/10.1080/00207217.2022.2068664

[5] Choi, Y.-S., Hong, J.-H., and Woo, J.-M. (2020). *Electrically and frequency-tunable printed inverted-F antenna with a perturbed parasitic element*. Journal of Electromagnetic Engineering and Science, 20(3), 164–170. https://doi.org/10.26866/jees.2020.20.3.164

[6] Zhang, X., and Zhao, A. (2009). Enhanced-bandwidth PIFA antenna with a slot on the ground plane. PIERS Proceedings, Beijing, China, pp. 1268–1272.

[7] Qi, Z., Ding, X., Yang, W., and Chen, J. (2022). *A compact broadband planar inverted-F antenna with dual-resonant modes*. Applied Sciences, 12(17), 8915. https://doi.org/10.3390/app12178915

[8] A Compact 2.4 GHz L-Shaped Microstrip Patch Antenna for ISM-Band Internet of Things (IoT) Applications. *Electronics*, 12(9), 2023, 1–12. https://doi.org/10.3390/electronics12092149

[9] Matin, M. A., and Sharif, M. S. (2025). Design strategies and performance of IoT antennas: A review. Wireless Personal Communications. https://doi.org/10.1007/s10791-025-09536-y

[10] Morabito, A. F. (2024). Antenna systems for IoT applications: A review. International Journal of RF and Microwave Computer-Aided Engineering, 34(1). https://doi.org/10.1002/mmce.23534

[11] Jadhav, T., Walekar, N., and Lakade, N. (2024). Metamaterial based PIFA antenna using defective ground surface for handheld applications. International Advanced Research Journal in Science, Engineering and Technology, 11(Special Issue 1).

[12] D. Mair and D. Baumgarten (2024). Evolutionary optimisation of pixelated IFA inspired antennas. Scientific Reports, 14, 77695. https://doi.org/10.1038/s41598-024-77695-x

[13] A Compact 2.4 GHz L-Shaped Microstrip Patch Antenna for ISM-Band Internet of Things (IoT) Applications. *Electronics*, 12(9), 2023, 1–12. https://doi.org/10.3390/electronics12092149

[14] A. Bou-el-harmel, M. Ouremchi, A. El Makhloufi, J. Belkadid, and S. Lakrit (2026). A compact 3D quasi-isotropic antenna for 2.4 GHz IoT sensors. AEUE - International Journal of Electronics and Communications, Article 156297. https://doi.org/10.1016/j.aeue.2026.156297

[15] Elias, B. B. Q., Soh, P. J., Al-Hadi, A. A., Akkaraekthalin, P., and Vandenbosch, G. A. E. (2021). *Bandwidth optimization of a textile PIFA with DGS using characteristic mode analysis*. Sensors, 21(7), 2516. https://doi.org/10.3390/s21072516

[16] Mrnka, M., Vašina, P., Kufa, M., Hebelka, V., and Raida, Z. (2016). *RF energy harvesting antennas operating in commercially deployed frequency bands: A comparative study*. International Journal of Antennas and Propagation, 2016, Article ID 7379624. https://doi.org/10.1155/2016/7379624